Mutations in the Katnb1 gene cause left-right asymmetry and heart defects

Furtado, M.B.[1,2*]; Merriner, D.J.[3,4]; Berger, S.[2]; Rhodes, D.[3]; Jamsai, D.[3], O'Bryan, M.K[3,4*].

[1.] The Jackson Laboratory, Bar Harbor, Maine, USA; 2. Australian Regenerative Medicine Institute, Monash University, Melbourne, Australia; [3]The Development and Stem Cells Program of Monash Biomedicine Discovery Institute and The Department of Anatomy and Developmental Biology, Monash University, Melbourne, Australia. [4]The School of Biological Sciences, Monash University, Melbourne, Australia.

***Corresponding authors:**

1. Prof. Moira K. O'Bryan

E: moira.obryan@monash.edu

2. Dr. Milena B. Furtado

E: milena.furtado@jax.org

Keywords: cilia, Katnb1, heart, development, katanin, microtubules

Abstract

Background: The microtubule-severing protein complex katanin is composed two subunits, the ATPase subunit, KATNA1, and the non-catalytic regulatory subunit, KATNB1. Recently, the *Katnb1* gene has been linked to infertility, regulation of centriole and cilia formation in fish and mammals, as well as neocortical brain development. KATNB1 protein is expressed in germ cells in humans and mouse, mitotic/meiotic spindles and cilia, although the full expression pattern of the *Katnb1* gene has not been described. Results: Using a knockin-knockout mouse model of *Katnb1* dysfunction we demonstrate that *Katnb1* is ubiquitously expressed during embryonic development, although a stronger expression is seen in the crown cells of the gastrulation organizer, the murine node. Furthermore, null and hypomorphic *Katnb1* gene mutations show a novel correlation between *Katnb1* dysregulation and the development of impaired left-right signaling, including cardiac malformations. Conclusion: Katanin function is a critical regulator of heart development in mice. These findings are potentially relevant to human cardiac development.

Introduction

Mutations in ciliary genes can induce pleiotropic phenotypes collectively referred to as ciliopathies. The dysfunction of the cellular cilium, a hair-like organelle that protrudes out of the cell surface, can cause severe malformations during embryonic development, including polydactyly, retinitis pigmentosa, the Bardet-Biedl and Joubert syndromes, and left-right abnormalities, among others (Quinlan et al., 2008; Hildebrandt et al., 2011; O'Donnell et al., 2012; Li et al., 2015; Braun and Hildebrandt, 2016). Cilia are important sensors for external microenvironmental inputs to the cell, and also participate in motile function (Malicki and Johnson, 2017). The core of cilia is composed of a microtubule-based structure called the axoneme, which is composed of a 9+2 microtubule arrangement (motile cilia, such as in the trachea and in the sperm tail) or 9+0 organization (primary cilia), depending on the presence of a central pair of microtubules and dynein arms on the outer microtubules. During gastrulation, the murine organizer node tissue is known to display diverse sets of monocilia that can promote unidirectional vesicular/molecular flow (nodal flow) or sense external mechanical/molecular signals that culminate in the transfer of asymmetric gene expression to the left lateral plate mesoderm (Komatsu and Mishina, 2013; Blum et al., 2014). The lateral plate mesodermal tissue gives rise to thoracic and abdominal organs, such as the heart and gut. The asymmetric signaling system activates the *Nodal* and *Pitx2* genes, which are responsible for patterning of many internal organs (Komatsu and Mishina, 2013; Blum et al., 2014). Therefore, ciliary gene disruptions have been shown to affect left-right signaling, and notably cardiac morphogenesis in mouse and humans (Komatsu and Mishina, 2013; Blum et al., 2014; Harrison et al., 2016). As evidence of the importance of cilia in heart development, a recent recessive forward genetic screen performed during murine fetal development revealed a high number of cilia-related genes involved in congenital heart disease, including genes involved in cilia-transduced cell signaling, ciliary vesicular trafficking and cilia-transduced cell signaling (Quinlan et al., 2008; Fakhro et al., 2011; Komatsu and Mishina, 2013; Blum et al., 2014; Li et al., 2015; Harrison et al., 2016). Among the cardiac phenotypes and mutations associated with ciliary defects were those that

lead to single great artery, ventricular septal defect (VSD), heterotaxy (random rearrangement of internal organs) or dextrocardia (heart positioned to the right of thoracic cavity, as opposed to the normal left-sided positioning), side by side rearrangement of the aorta and pulmonary arteries; double outlet right ventricle (DORV) and atrioventricular septal defect (AVSD), among others. Such mutations are also consistent with murine deletions in the *Pitx2* gene (Kitamura et al., 1999; Liu et al., 2002; Tessari et al., 2008; Ma et al., 2013).

The katanin complex participates in microtubule severing and has been previously identified as a regulator of mammalian cilia formation (both motile and primary cilia) and other microtubular structures (Hartman and Vale, 1999; O'Donnell et al., 2012). While the katanin KATNA1 subunit displays catalytic activity and is the effector protein within the complex, KATNB1 serves to modestly enhance severing activity, but more importantly define severing specificity (Hartman and Vale, 1999; Roll-Mecak and McNally, 2010). N-terminal and missense mutations, as well as loss of function of *KATNB1* in patients are causative of cerebral malformations, presumably through limiting centriole and cilia number (Hu et al., 2014), disruption of mitotic spindle formation and consequent neuroblast formation and dendritic arborization (Mishra-Gorur et al., 2014), but the role of KATNB1 in cardiovascular abnormalities is so far unexplored. Here we reveal that mice carrying an N-terminal truncated homozygous mutation in the *Katnb1* gene (*Katnb1*$^{-}$) do not survive embryonic development and display an array of embryonic malformations consistent with disturbances in the left-right signaling pathway. A second allelic combination (*Katnb1*$^{-/Taily}$) further revealed cardiac abnormalities. Our findings will be important to guide future screening and diagnosis of patients showing mutations in the *Katnb1* gene.

Results

Katnb1 is ubiquitously expressed throughout embryonic development.

Katnb1 expression has been previously reported in the murine and human testis (O'Donnell et al., 2012; Pleuger et al., 2016), cerebral cortex during mouse, human and zebrafish development (Hu et al., 2014; Mishra-Gorur et al., 2014) and developing heart (Yu et al., 2005). Due to the insertion of a beta-galactosidase reporter cassette in our *Katnb1* recombination locus, we were able to detect LacZ activity in *Katnb1*$^{+/-}$ embryos (Figure 1; Figure S1), and therefore infer *Katnb1* gene expression throughout embryonic development through expression of LacZ. While *Katnb1* expression was ubiquitous from early developmental stages, enriched expression was found in the gastrulating nodal tissue (Figure 1A) and primitive streak from 6.5 days *post-coitum* (dpc). Node staining was sustained from 7.5 dpc to 8.5dpc (Figure 1B-E), stages when the cardiac mesoderm is deployed in the embryo and the break of molecular symmetry at the node is established. At 7.5 dpc, strong *Katnb1* expression was observed in the node pit and crown cells (Figure 1B', C, D) and weakly in the cardiac crescent region of the embryo (cc – Figure 1B). At 8.5dpc, staining was visible in the midline and node areas (Figure 1E, E', E"), both of which are important for the establishment of left-sided Nodal and Pitx2 signaling during left-right establishment in the early embryo (Furtado et al., 2008; Komatsu and Mishina, 2013). When embryos were stained for longer periods of time (Figure 1F), ubiquitous expression throughout the body, including the looping heart (H), brain and allantois regions were observed. This expression pattern was confirmed using *in situ* hybridization (data not shown), that showed ubiquitous *Katnb1* anti-sense probe staining at 8.5dpc. This ubiquitous pattern of expression was retained at later stages of development (Figure 1 G-K). In the heart, LacZ staining was seen in all cardiac segments, including atria (A), ventricles (V) and outflow tract (OT), cardiac cushions in OT and atrioventricular canal areas (* in Figure 1J). These data suggest that *Katnb1* may affect cilia/microtubule signaling in every single cell type of the developing embryo, but in particular, the left-right asymmetry establishing tissues, and the heart.

Katnb1$^{-/-}$ mutants show growth retardation and are embryonically lethal.

To determine whether *Katnb1*$^{-/-}$ mice displayed an embryonic phenotype, *Katnb1*$^{+/-}$ adults were intercrossed for timed matings and embryos were collected at various developmental stages, from 8.5 post-coitum (dpc) to birth. *Katnb1*$^{-/-}$ mutant embryos showed expected Mendelian inheritance ratios (Table 1) when compared with *Katnb1*$^{+/-}$ or *Katnb1*$^{+/+}$ littermates from 8.5 to 11.5 dpc (Table 1). At 12.5dpc, the obtained number of *Katnb1*$^{-/-}$ mutants was below expectations. Visual and histological analysis of *Katnb1*$^{-/-}$ embryos at these ages revealed severe growth retardation, combined with brain and other abnormalities (Table 1 and Figure 2). Our observations are consistent with findings from a previously described *Katnb1* gene-trap mouse model (Hu et al., 2014).

Katnb1$^{-/-}$ mutants display defects consistent with abnormal establishment of left-right asymmetry.

Due to the enhanced expression of *Katnb1* in the node and midline structures during gastrulation and links between KATNB1 in other tissues and species (Figure 1), we investigated whether *Katnb1* mutant embryos showed any signs of left-right axis patterning abnormalities. At 10.5 dpc, *Katnb1*$^{-/-}$ mutant embryos showed a range of axial distortions that shifted heart positioning to the left side of the body, as opposed to the normal midline positioning (Figure 2 - red solid lines in A, E, I, M', R') when compared with control *Katnb1*$^{+/+}$ and *Katnb1*$^{+/-}$ embryos. Because early left-right Nodal signaling impacts midline formation, axial distortions are seen in *Pitx2* mutant embryos (Gage et al., 1999; Kitamura et al., 1999; Furtado, 2008; Furtado et al., 2011), consistent with our findings. Heart looping was also abnormal in some embryos I-L, M-Q, R-V. Heart looping varied for normal configuration (insets in A', E') to partial configurations (I-L, R-V), in which the LV and RV adopt abnormal positioning in relation to each other (highlighted by insets in I', M', R'). In addition, tail positioning was altered in *Katnb1*$^{-/-}$ mutants (Figure 2 – dashed black lines in A", E", I", M' and R'), forming a V-shape figure as opposed to the normal O-shaped tail loop in normal embryos. Despite

the abnormal tail positioning, only 1 in 23 *Katnb1*$^{-/-}$ mutant embryo showed inverted tail looping (Figure 2R). All these abnormalities are consistent with disturbances in the left-right pathway (Gage et al., 1999; Kitamura et al., 1999; Furtado, 2008; Furtado et al., 2011).

Katnb1*$^{-/Taily}$ *mutants show range of heart abnormalities.

Due to the limitations imposed by the early embryonic lethality of *Katnb1*$^{-/-}$ embryos, we subsequently used an allelic series strategy to investigate whether KATNB1 function is also required heart remodelling. For these experiments, we crossed heterozygous *Katnb1*$^{+/-}$ with *Katnb1*$^{+/Taily}$ animals, which contained a hypomorphic point-mutation in the *Katnb1* gene (O'Donnell et al., 2012). Fetuses were collected for cardiac analyses at 16.5 dpc, a stage when heart remodeling is normally complete in the mouse. While control animals (*Katnb1*$^{+/+}$; *Katnb1*$^{+/-}$; *Katnb1*$^{+/Taily}$) showed normal growth and heart morphology (Table 2; Figure 3A, A'), compound heterozygous animals (*Katnb1*$^{-/Taily}$) were growth retarded as indicated by smaller body and head sizes (Figure 3 G, M, S). Heart sizes were grossly normal in *Katnb1*$^{-/Taily}$ mutants (Figure 3 G', M'), apart from 1/9 severely hypoplastic heart (Figure 3 S'). Histological analysis, however, revealed differential penetrance of a range of cardiac remodeling abnormalities in *Katnb1*$^{-/Taily}$ compound mutant hearts. Defects included atrial septal defects (2/9; Table 2 and green dashed circle in Figure 3Q, X), ventricular septal defects (2/9; Table 2 and green dashed circle in Figure 3W), myocardial thinning (3/9; Table 2 and green brackets in Figure 3O, U). In some hearts, the aorta and pulmonary artery were visibly rooted in the right ventricle, while there was a lack of fibrous continuity between the aortic and mitral valves, consistent with a double outlet right ventricle (2/9; Table 2 and blue/red arrows in Figure 3T-V). These data establish KATNB1 function as an essential requirement for embryogenesis and notably, heart formation. These defects are consistent with the cardiac phenotype displayed by mutations in other ciliary genes (Fakhro et al., 2011; Li et al., 2015; Braun and Hildebrandt, 2016; Harrison et al., 2016) and the left-right main effector gene *Pitx2* (Gage et al., 1999; Kitamura et al., 1999; Liu et al., 2002; Tessari et al., 2008; Ma et al., 2013).

Discussion

Apart from one study demonstrating the presence of katanin p60 and p80 in rat and murine embryonic and adult tissues, detailed katanin p80 expression has not been described (Yu et al., 2005). Both katanin subunits were found in rat embryos from 15 dpc to adulthood using western blots. Protein expression was further defined in heart and brain tissue in rat and mouse using western blot and immunohistochemistry, respectively (Yu et al., 2005). We used a lacZ reporter cassette insertion into the *Katnb1* locus (Fig. S1) to track expression of the *Katnb1* gene. LacZ expression was ubiquitous from early development (8.5 dpc). Under-staining of early embryos revealed regions of increased LacZ, and thus *Katnb1*, expression, including the node and midline structures, suggesting a potentially unknown role for *Katnb1* in left-right asymmetry formation. Indeed, we encountered a series of so far unnoticed early and late hallmarks of left-right signaling phenotypes in *Katnb1* mutant embryos, including heart/tail looping, axial abnormalities and later cardiac malformations. Due to the many other abnormalities shown in mutant embryos early in development, including growth retardation, we cannot discard the possibility that the observed left-right abnormalities are secondary to impaired growth. In combination with the LacZ staining, reflecting *Katnb1* expression, in the node area this data is, however, strongly suggestive of a primary left-right patterning phenotype.

Strong genetic evidence links a broad range of ciliopathies to laterality disturbances. Murine models have been at the forefront of discovery and modeling of such syndromes (Norris and Grimes, 2012). The Kartagener's syndrome, as subgroup of primary ciliary dyskinesia (PCD), was amongst the first to demonstrate a correlation between *situs inversus*, heterotaxy and congenital heart disease with other phenotypes related to cilia dysfunction, such as bronchiectasis and male infertility (Leigh et al., 2009). PCD is associated with mutations of dynein protein components, amongst others, in patients (Lancaster and Gleeson, 2009). Other syndromes that show involvement of left-right asymmetry defects include polycystic kidney disease (Harris and Torres, 2009; Bataille et al., 2011; Onoe et al.,

2013), Bardet-Biedl (Lorda-Sanchez et al., 2000; Tobin and Beales, 2007), Meckel-Gruber (Norris and Grimes, 2012), Joubert syndrome (Louie and Gleeson, 2005), nephronophthisis (Hoff et al., 2013) and orofaciodigital syndrome (Ferrante et al., 2006) wherein a broad range of brain and heart malformations have been reported.

The commonality among ciliopathy phenotypes associated with laterality defects derives from the importance of the ciliated node, the gastrulation organizer during in early embryonic development (Komatsu and Mishina, 2013). The transient molecular flow generated by cilia movement at the node is essential for the asymmetric formation of most thoracic and abdominal organs, including the heart. In fact, asymmetric heart formation, usually measured by early looping, is a hallmark for the presence of left-right defects (Furtado et al., 2011; Komatsu and Mishina, 2013). Heart looping takes place at around 8.5 dpc in mouse development and is important for the proper alignment of all cardiac chambers to their final configuration seen in the adult heart, since hearts at earlier embryonic stages are arranged in a linear fashion (Brand, 2003). Other signs of left-right disturbances include abnormal tail looping and axial disturbances (Kitamura et al., 1999; Lu et al., 1999; Furtado et al., 2011). In this study, *Katnb1*$^{-/-}$ embryos showed a range of partially penetrant left-right phenotypes detected at early developmental stages, including abnormal or inverted heart and tail looping, and axial distortions. Such defects are consistent with defects in left-right pathway genes, including the main effector of the Nodal pathway, the transcription factor *Pitx2* (Kitamura et al., 1999; Lu et al., 1999; Furtado et al., 2011). *Katnb1*$^{-/-}$ embryos also displayed severe growth retardation and neural tube defects as previously described (Hu et al., 2014; Mishra-Gorur et al., 2014), once again consistent with various ciliopathy syndromes (Lorda-Sanchez et al., 2000; Louie and Gleeson, 2005; Ferrante et al., 2006; Tobin and Beales, 2007; Harris and Torres, 2009; Lancaster and Gleeson, 2009; Leigh et al., 2009; Bataille et al., 2011; Norris and Grimes, 2012; Hoff et al., 2013; Onoe et al., 2013). Although *Katnb1*$^{-/-}$ embryos could not be found at late fetal stages, the allelic series (*Katnb1*$^{-/Taily}$) used in this study allowed us to investigate heart formation at later developmental time points, when heart morphogenesis is complete. *Katnb1*$^{-/Taily}$ animals did not

show gross growth retardation but presented with a series of heart malformations, including atrial and ventricular septal defects, hypoplasticity of chambers and double outlet right ventricle, once again in a partial penetrant fashion. These defects are also found in *Pitx2* mutant embryos (Gage et al., 1999; Kitamura et al., 1999; Liu et al., 2002; Tessari et al., 2008; Furtado et al., 2011; Ma et al., 2013). Interestingly, mouse genetic models have been proved useful to detect partially penetrant phenotypes not always obvious in patient screenings (Norris and Grimes, 2012), and we believe this to be the case for the *Katnb1* gene. Previous mutation screenings have identified a role for *KATNB1* in brain development in humans (Hu et al., 2014; Mishra-Gorur et al., 2014), but have not explored heart formation. While we would predict severe heart defects in humans containing the equivalent genetic variants, as for all syndromic ciliopathies, phenotype penetrance is variable (Hu et al., 2014; Mishra-Gorur et al., 2014). In summary, our data highlights the usefulness of murine genetic models in the phenotypic dissection of ciliopathy genes.

Experimental Procedures

Mouse handling

Mice were housed at the Monash University Animal Services laboratories. The investigation conforms to the Guide for the Care and Use of Laboratory Animals published by the US National Institutes of Health (NIH Publication No. 85–23, revised 1996) and the National Health and Medical Research Council of Australia and with requirements under the ethics application MARP/2013/069 (Monash University).

Generation of *Katnb1* mouse lines

The *Katnb1* knockout mouse line was generated at the Australian Phenomics Network (APN) Monash University Node using a EUCOMM KO-first condition ready ES clone (HEPD0636_3_G09) using standard methods (Cotton et al., 2015). To disrupt the *Katnb1* gene (ENSMUSG00000031787), the FRT-LacZ-loxP-Neo-FRT-loxP-*Katnb1-exon4*-loxP cassette was inserted in intron 3 of the *Katnb1* gene ($Katnb1^{tm1a(EUCOMM)Hmgu}$ allele). In the absence of FLP or CRE recombinase deletions, this knockin allele resulted in truncated mRNA containing exons 1-3 (ENSMUSE00000606263, ENSMUSE00000446632, ENSMUSE00000212971), encoded the first 57 N-terminal amino acids of the protein (Figure 4). The $Katnb1^{tm1a(EUCOMM)Hmgu}$ allele has been shortened $Katnb1^{-}$ in this manuscript.

Heterozygous knockout mice ($Katnb1^{-/+}$) mice were also intercrossed with another *Katnb1* mutant mouse line, *Taily*, which carries a hypomorphic V to F point-mutation in exon 8 of the *Katnb1* gene (O'Donnell et al., 2012) to produce compound heterozygous ($Katnb1^{-/Taily}$) progeny. Mouse genotypes from tail biopsies were determined using real time PCR with specific probes designed for each allele (Transnetyx, Cordova, TN) (Table S1).

Time mating and embryo analysis

Heterozygous knockout mice were timed mated for the collection of embryos at various time points (8.5 to 18.5dpc). Whole mount images of embryos were obtained using the Olympus SZX16 stereo dissecting microscope. For histological analyses, embryos were fixed overnight in 4% paraformaldehyde, dehydrated through an ethanol series (25%, 50%, 75% and twice 100%), followed by two xylene washes and 3 paraffin changes (Leica). Embryos were paraffin embedded, sectioned at 8-10 μm in a Leica microtome, dewaxed and mounted using DEPEX mounting media. Slides were scanned using the Aperio Scanscope AT Turbo at the Monash Histology Platform.

Beta-Galactosidase (lacZ) Staining

Embryos were dissected and immediately fixed for 10 min in 1% formaldehyde and 0.2% glutaraldehyde in X-gal buffer (5mM EGTA, 2mM $MgCl_2$, 0.02% IGEPAL, 24μM deoxycholate in PBS); washed and stained in X-gal staining solution (5 mM $K_3Fe(CN)_6$; 5 mM $K_4Fe(CN)_6.3H_2O$; 0.5 mg/ml X-gal in X-gal buffer) overnight at 37^{o}C. Following staining development, embryos were again washed in X-gal buffer and stored in 4% PFA.

Acknowledgments: The authors acknowledge the facilities and scientific and technical assistance of Monash Micro Imaging and Histology Platforms, Monash University.

Competing interests: no competing interests declared.

Funding: This work was supported in part by a National Health and Medical Research Council (NHMRC) grant to MKOB (APP1020753). MKOB was funded by an NHMRC fellowship (APP1058356).

References:

Bataille S, Demoulin N, Devuyst O, Audrezet MP, Dahan K, Godin M, Fontes M, Pirson Y, Burtey S. 2011. Association of PKD2 (polycystin 2) mutations with left-right laterality defects. Am J Kidney Dis 58:456-460.

Blum M, Schweickert A, Vick P, Wright CV, Danilchik MV. 2014. Symmetry breakage in the vertebrate embryo: when does it happen and how does it work? Dev Biol 393:109-123.

Brand T. 2003. Heart development: molecular insights into cardiac specification and early morphogenesis. Dev Biol 258:1-19.

Braun DA, Hildebrandt F. 2016. Ciliopathies. Cold Spring Harb Perspect Biol.

Cotton LM, Meilak ML, Templeton T, Gonzales JG, Nenci A, Cooney M, Truman D, Rodda F, Lynas A, Viney E, Rosenthal N, Bianco DM, O'Bryan MK, Smyth IM. 2015. Utilising the resources of the International Knockout Mouse Consortium: the Australian experience. Mamm Genome 26:142-153.

Fakhro KA, Choi M, Ware SM, Belmont JW, Towbin JA, Lifton RP, Khokha MK, Brueckner M. 2011. Rare copy number variations in congenital heart disease patients identify unique genes in left-right patterning. Proc Natl Acad Sci U S A 108:2915-2920.

Ferrante MI, Zullo A, Barra A, Bimonte S, Messaddeq N, Studer M, Dolle P, Franco B. 2006. Oral-facial-digital type I protein is required for primary cilia formation and left-right axis specification. Nat Genet 38:112-117.

Furtado MB. 2008. Impact of Asymmetric Signalling Pathways on the Mouse Heart Development. In: St Vincent's School of Medicine: University of New South Wales.

Furtado MB, Biben C, Shiratori H, Hamada H, Harvey RP. 2011. Characterization of Pitx2c expression in the mouse heart using a reporter transgene. Dev Dyn 240:195-203.

Furtado MB, Solloway MJ, Jones VJ, Costa MW, Biben C, Wolstein O, Preis JI, Sparrow DB, Saga Y, Dunwoodie SL, Robertson EJ, Tam PP, Harvey RP. 2008. BMP/SMAD1 signaling sets a threshold for the left/right pathway in lateral plate mesoderm and limits availability of SMAD4. Genes Dev 22:3037-3049.

Gage PJ, Suh H, Camper SA. 1999. Dosage requirement of Pitx2 for development of multiple organs. Development 126:4643-4651.

Harris PC, Torres VE. 2009. Polycystic kidney disease. Annu Rev Med 60:321-337.

Harrison MJ, Shapiro AJ, Kennedy MP. 2016. Congenital Heart Disease and Primary Ciliary Dyskinesia. Paediatr Respir Rev 18:25-32.

Hartman JJ, Vale RD. 1999. Microtubule disassembly by ATP-dependent oligomerization of the AAA enzyme katanin. Science 286:782-785.

Hildebrandt F, Benzing T, Katsanis N. 2011. Ciliopathies. N Engl J Med 364:1533-1543.

Hoff S, Halbritter J, Epting D, Frank V, Nguyen TM, van Reeuwijk J, Boehlke C, Schell C, Yasunaga T, Helmstadter M, Mergen M, Filhol E, Boldt K, Horn N, Ueffing M, Otto EA, Eisenberger T, Elting MW, van Wijk JA, Bockenhauer D, Sebire NJ, Rittig S, Vyberg M, Ring T, Pohl M, Pape L, Neuhaus TJ, Elshakhs NA, Koon SJ, Harris PC, Grahammer F, Huber TB, Kuehn EW, Kramer-Zucker A, Bolz HJ, Roepman R, Saunier S, Walz G, Hildebrandt F, Bergmann C, Lienkamp SS. 2013. ANKS6 is a central component of a nephronophthisis module linking NEK8 to INVS and NPHP3. Nat Genet 45:951-956.

Hu WF, Pomp O, Ben-Omran T, Kodani A, Henke K, Mochida GH, Yu TW, Woodworth MB, Bonnard C, Raj GS, Tan TT, Hamamy H, Masri A, Shboul M, Al Saffar M, Partlow JN, Al-Dosari M, Alazami A, Alowain M, Alkuraya FS, Reiter JF, Harris MP, Reversade B, Walsh CA. 2014. Katanin p80 regulates human cortical development by limiting centriole and cilia number. Neuron 84:1240-1257.

Kitamura K, Miura H, Miyagawa-Tomita S, Yanazawa M, Katoh-Fukui Y, Suzuki R, Ohuchi H, Suehiro A, Motegi Y, Nakahara Y, Kondo S, Yokoyama M. 1999. Mouse Pitx2 deficiency leads to anomalies of the ventral body wall, heart, extra- and periocular mesoderm and right pulmonary isomerism. Development 126:5749-5758.

Komatsu Y, Mishina Y. 2013. Establishment of left-right asymmetry in vertebrate development: the node in mouse embryos. Cell Mol Life Sci 70:4659-4666.

Lancaster MA, Gleeson JG. 2009. The primary cilium as a cellular signaling center: lessons from disease. Curr Opin Genet Dev 19:220-229.

Leigh MW, Pittman JE, Carson JL, Ferkol TW, Dell SD, Davis SD, Knowles MR, Zariwala MA. 2009. Clinical and genetic aspects of primary ciliary dyskinesia/Kartagener syndrome. Genet Med 11:473-487.

Li Y, Klena NT, Gabriel GC, Liu X, Kim AJ, Lemke K, Chen Y, Chatterjee B, Devine W, Damerla RR, Chang C, Yagi H, San Agustin JT, Thahir M, Anderton S, Lawhead C, Vescovi A, Pratt H, Morgan J, Haynes L, Smith CL, Eppig JT, Reinholdt L, Francis R, Leatherbury L, Ganapathiraju MK, Tobita K, Pazour GJ, Lo CW. 2015. Global genetic analysis in mice unveils central role for cilia in congenital heart disease. Nature 521:520-524.

Liu C, Liu W, Palie J, Lu MF, Brown NA, Martin JF. 2002. Pitx2c patterns anterior myocardium and aortic arch vessels and is required for local cell movement into atrioventricular cushions. Development 129:5081-5091.

Lorda-Sanchez I, Ayuso C, Ibanez A. 2000. Situs inversus and hirschsprung disease: two uncommon manifestations in Bardet-Biedl syndrome. Am J Med Genet 90:80-81.

Louie CM, Gleeson JG. 2005. Genetic basis of Joubert syndrome and related disorders of cerebellar development. Hum Mol Genet 14 Spec No. 2:R235-242.

Lu MF, Pressman C, Dyer R, Johnson RL, Martin JF. 1999. Function of Rieger syndrome gene in left-right asymmetry and craniofacial development. Nature 401:276-278.

Ma HY, Xu J, Eng D, Gross MK, Kioussi C. 2013. Pitx2-mediated cardiac outflow tract remodeling. Dev Dyn 242:456-468.

Malicki JJ, Johnson CA. 2017. The Cilium: Cellular Antenna and Central Processing Unit. Trends Cell Biol 27:126-140.

Mishra-Gorur K, Caglayan AO, Schaffer AE, Chabu C, Henegariu O, Vonhoff F, Akgumus GT, Nishimura S, Han W, Tu S, Baran B, Gumus H, Dilber C, Zaki MS, Hossni HA, Riviere JB, Kayserili H, Spencer EG, Rosti RO, Schroth J, Per H, Caglar C, Caglar C, Dolen D, Baranoski JF, Kumandas S, Minja FJ, Erson-Omay EZ, Mane SM, Lifton RP, Xu T, Keshishian H, Dobyns WB, Chi NC, Sestan N, Louvi A, Bilguvar K, Yasuno K, Gleeson JG, Gunel M. 2014. Mutations in KATNB1 cause complex cerebral malformations by disrupting asymmetrically dividing neural progenitors. Neuron 84:1226-1239.

Norris DP, Grimes DT. 2012. Mouse models of ciliopathies: the state of the art. Dis Model Mech 5:299-312.

O'Donnell L, Rhodes D, Smith SJ, Merriner DJ, Clark BJ, Borg C, Whittle B, O'Connor AE, Smith LB, McNally FJ, de Kretser DM, Goodnow CC, Ormandy CJ, Jamsai D, O'Bryan MK. 2012. An essential role for katanin p80 and microtubule severing in male gamete production. PLoS Genet 8:e1002698.

Onoe T, Konoshita T, Tsuneyama K, Hamano R, Mizushima I, Kakuchi Y, Yamada K, Hayashi K, Kuroda M, Kagitani S, Nomura H, Yamagishi M, Kawano M. 2013. Situs inversus and cystic kidney disease: Two adult patients with this Heterogeneous syndrome. Am J Case Rep 14:20-25.

Pleuger C, Fietz D, Hartmann K, Weidner W, Kliesch S, O'Bryan MK, Dorresteijn A, Bergmann M. 2016. Expression of katanin p80 in human spermatogenesis. Fertil Steril 106:1683-1690 e1681.

Quinlan RJ, Tobin JL, Beales PL. 2008. Modeling ciliopathies: Primary cilia in development and disease. Curr Top Dev Biol 84:249-310.

Roll-Mecak A, McNally FJ. 2010. Microtubule-severing enzymes. Curr Opin Cell Biol 22:96-103.

Tessari A, Pietrobon M, Notte A, Cifelli G, Gage PJ, Schneider MD, Lembo G, Campione M. 2008. Myocardial Pitx2 differentially regulates the left atrial identity and ventricular asymmetric remodeling programs. Circ Res 102:813-822.

Tobin JL, Beales PL. 2007. Bardet-Biedl syndrome: beyond the cilium. Pediatr Nephrol 22:926-936.

Yu W, Solowska JM, Qiang L, Karabay A, Baird D, Baas PW. 2005. Regulation of microtubule severing by katanin subunits during neuronal development. J Neurosci 25:5573-5583.

Figure legends

Figure 1 – *Katnb1* expression in embryonic development reported by LacZ activity. A. Ventral view of a 6.5dpc embryo showing pale ubiquitous staining throughout embryo and stronger staining in the node and primitive streak areas. B. Ventral view of 7.5 dpc embryo showing pale staining in cardiac crescent (cc) area, highlighted by dashed black line, and node (boxed area). B' zoom of nodal staining. C-D. Histological sections through crown cells on the node (C) and pit region (D). E-E". Ventral view of 8.5 dpc embryo highlighting midline (E') and node (E") staining in boxed regions. F. Overnight staining of 8.5 dpc embryo highlighted the ubiquitous embryonic LacZ staining, including the heart (H). G. Ubiquitous staining was sustained to 9.5 dpc. H. Sagittal section showing ubiquitous LacZ staining in the neural tube (NT), outflow tract (OT), ventricle (V) and atrial (A) cardiac regions. I-K. Lateral views of 11.5 dpc embryo, showing ubiquitous LacZ staining was sustained at later developmental stages. J. Isolated 11.5 dpc heart showed staining in all compartments. K. Sagittal section highlighting staining in branchial arch (BA), and heart (H), including cardiac cushion material (asterisks), responsible for formation of valves and for septation.

Figure 2 – *Katnb1*$^{-/-}$ embryos showed developmental delay, turning and heart looping phenotypes at 10.5dpc. A-D. Ventral (A), left-sided (A') and right-sided (A") views of control embryo showing normal development of neural tube, body axis (red line), heart (black dashed circle) and tail positioning (black dashed lines). B-D. Sagittal sections through various levels of the heart showing proper formation and positioning of cardiac chambers, including left ventricle (LV), right ventricle (RV), atrioventricular canal (AVC), atria (A), sinus venosus (SV) and outflow tract (OT). E-H. Mutant embryo displaying growth retardation (E-E"), axis (E) and tail looping (E") abnormalities but grossly normal heart looping (E', F-H). I-L. Mutant embryo showing intermediate axial (I), heart (I', J-L) and tail looping (I") abnormalities. M-V. Two mutant embryos showing

severe growth retardation (M, R) and other morphogenetic defects. Closer ventral view of embryos (M', R') highlights axial rotation, as well as abnormal heart and tail looping. N-Q. Ventral sections of mutant embryo shown in M, displaying looping abnormalities. R-V. Sagittal sections through embryo shown in R, showing abnormal alignment of cardiac chambers. Insets in A', E',I',M and R show orientation of the RV in relation to the LV. A' shows correct relationship between ventricles. *Katnb*$^{-/-}$ muatn embryos show a range of looping phenotypes from correct heart loop (E') or partial heart loops (I', R) to reversal (M').

B – brain; T – tail.

Figure 3 – *Katnb1*$^{-/Taily}$ compound fetuses show cardiac abnormalities at 16.5 dpc. A, G, M, S - Head sizes highlight growth retardation in *Katnb1*$^{-/Taily}$ fetuses when compared with control littermates. The genotype is indicated on the left hand side of the figure. A', G', M', S' - Whole mount view of control and compound mutant hearts (*Katnb1*$^{-/Taily}$) showing the gross morphology was not affected in most hearts. B-X - Longitudinal sections of hearts showing partially penetrant cardiac malformations in compound mutant fetuses. The range in the severity of phenotype is shown from top to bottom panels, with less severe on top (H-L). Hearts shown in panels S'-X had the most severe phenotype, consisting of double outlet right ventricle (DORV), ventricular septal defect (VSD; dashed area and inset in W) and atrial septal defect (ASD; dashed area and inset in Q, X). The blue arrows point to the direction of connection of the right ventricle (RV) with the pulmonary artery. The red arrows point to the direction of the connection between the left ventricle (LV) with the aorta, or the RV with the aorta in panel U. Dashed areas and insets in N, X point to malformed atrial or W for ventricular septa. Dashed area and inset in C show normal compact myocardium in control heart or highlights hypoplastic myocardial chambers in *Katnb1*$^{-/taily}$ mutant hearts (I, O and U). RA – right atrium; LA – left atrium

Figure 4 – Genetic map of *Katnb1* allelic series used for embryonic phenotyping. A. EUCOMM engineered allele showing Flp-recombinase recognition sites (FRT) flanking a beta-galactosidase expression cassette (lacZ) and a neomycin selection cassette (neo). Three Cre-recombinase recognition sites (LoxP) allow excision of the neo cassette and/or the endogenous exon4 of the *Katnb1* gene. FRT sites allow excision of lacZ and neomycin cassettes. The mice used in this manuscript have not undergone CRE or FLP mediated deletion, but the insertion of the knockin cassette causes premature termination of the gene. B. A second *Katnb1* allele ($Katnb1^{Taily}$) was independently modified by a point mutation in exon 8, which caused a G/T nucleotide change and conversion from valine to phenylalanine in the WD40 domain of the protein (O'Donnell et al., 2012), supposed to bind p60 and target the protein to subcellular compartments. This allele was further crossed with allele A ($Katnb1^{-}$).

Tables

Table 1 – Inheritance of the *Katnb1*$^{-}$ allele at various developmental stages.

	Total number of embryos	Genotype	Observed	Expected	Chi-square (p)*
8.5 dpc	**37**	***WT***	8	9.25	**0.676 (0.7133)**
		Het	21	18.5	
		Hom	8	9.25	
9.5 dpc	**22**	***WT***	6	5.5	**0.182 (0.9131)**
		Het	10	11	
		Hom	6	5.5	
10.5 dpc	**25**	***WT***	7	6.25	**2.28 (0.3198)**
		Het	9	12.5	
		Hom	9	6.25	
11.5 dpc	**28**	***WT***	11	7	**3.429 (0.1800)**
		Het	10	14	
		Hom	7	7	
12.5 dpc	**25**	***WT***	3	6.25	**6.76 (0.0340)**
		Het	19	12.5	
		Hom	3	6.25	
Term (P0)	**154**	***WT***	53	38.5	**51.44 (0)**
		Het	101	77	
		Hom	0	38.5	

*2 degrees of freedom (Preacher, K. J. 2001. Calculation for the chi-square test: An interactive calculation tool for chi-square tests of goodness of fit and independence [Computer software]. Available from http://quantpsy.org.)

Table 2 – *Katnb1*$^{+/-}$ x *Katnb1*$^{+/-}$ embryonic phenotyping

	Genotype	Affected	Normal	Affected (%)
Looping/Turning	***WT***	0	27	**0%**
	Het	3	49	**5.8%**
	Hom	16	7	**69.6%**
Growth Retardation	***WT***	1	26	**3.7%**
	Het	5	47	**9.6%**
	Hom	17	6	**73.9%**
Neural Tube Defect	***WT***	1	26	**3.7%**
	Het	0	52	**0%**
	Hom	11	12	**47.8%**

Table 3 – *Katnb1*$^{+/-}$ x *Katnb1*$^{+/Taily}$ cardiac phenotyping

	Genotype	Affected	Normal	Affected (%)
Myocardial thinning	***Katnb1*$^{-/Taily}$**	3	7	**30%**
	***Katnb1*$^{+/Taily}$**	0	9	**0%**
	***Katnb1*$^{+/-}$**	0	9	**0%**
	WT	0	2	**0%**
Atrial septal defect	***Katnb1*$^{-/Taily}$**	2	7	**28.9%**
	***Katnb1*$^{+/Taily}$**	0	9	**0%**
	***Katnb1*$^{+/-}$**	0	9	**0%**
	WT	0	2	**0%**
Ventricular septal defect	***Katnb1*$^{-/Taily}$**	2	7	**28.9%**
	***Katnb1*$^{+/Taily}$**	0	9	**0%**
	***Katnb1*$^{+/-}$**	0	9	**0%**
	WT	0	2	**0%**
Double outlet right ventricle	***Katnb1*$^{-/Taily}$**	2	7	**28.9%**
	***Katnb1*$^{+/Taily}$**	0	9	**0%**
	***Katnb1*$^{+/-}$**	0	9	**0%**
	WT	0	2	**0%**

Table Supplementary 1 – Primers used for genotyping

Allele	Assay name	Primers and probes
Taily	Katnb1-1	Forward Primer: GGTGGTGAGCTGCATTGAAG
	MUT	Reverse Primer: GAGCAGAGGCAGGGAAGAG
		Reporter 1: CGGGCCCGTCAGGTA
		Reporter 2: CCGGGCCCTTCAGGTA
Katnb1$^{KO/WT}$	Katnb1-2 WT	Forward Primer: CAATGTAGCAGCAGTGGTCACT
		Reverse Primer: ACACCTTACTCTTCATCCCTTGGA
		Reporter: ACCTCATGCCAGCAACT
	LAC Z	Forward Primer: CGATCGTAATCACCCGAGTGT
		Reverse Primer: CCGTGGCCTGACTCATTCC
		Reporter: CCAGCGACCAGATGAT
Katnb1$^{Flox/WT}$	Katnb1-2 WT	Forward Primer: CAATGTAGCAGCAGTGGTCACT
		Reverse Primer: ACACCTTACTCTTCATCCCTTGGA
		Reporter: ACCTCATGCCAGCAACT
	Katnb1-2 MD	Forward Primer: GCTGGCGCCGGAAC
		Reverse Primer: GCGACTATAGAGATATCAACCACTTTGT
		Reporter: AAGCTGGGTCTAGATATC
	LAC Z	Forward Primer: CGATCGTAATCACCCGAGTGT
		Reverse Primer: CCGTGGCCTGACTCATTCC
		Reporter: CCAGCGACCAGATGAT
Katnb1$^{Flox/Flox}$	Katnb1-2 WT	Forward Primer: CAATGTAGCAGCAGTGGTCACT
		Reverse Primer: ACACCTTACTCTTCATCCCTTGGA
		Reporter: ACCTCATGCCAGCAACT
	Katnb1-2 MD	Forward Primer: GCTGGCGCCGGAAC

		Reverse Primer: GCGACTATAGAGATATCAACCACTTTGT Reporter: AAGCTGGGTCTAGATATC
Katnb1$^{Flox/Del,\ Stra8\text{-}Cre+}$	Katnb1-2 WT	Forward Primer: CAATGTAGCAGCAGTGGTCACT Reverse Primer: ACACCTTACTCTTCATCCCTTGGA Reporter: ACCTCATGCCAGCAACT
	Katnb1-2 MD	Forward Primer: GCTGGCGCCGGAAC Reverse Primer: GCGACTATAGAGATATCAACCACTTTGT Reporter: AAGCTGGGTCTAGATATC
	CRE	Forward Primer: TTAATCCATATTGGCAGAACGAAAACG Reverse Primer: CAGGCTAAGTGCCTTCTCTACA Reporter: CCTGCGGTGCTAACC
Katnb1$^{Del/Del,\ Stra8\text{-}Cre+}$	Katnb1-2 WT	Forward Primer: CAATGTAGCAGCAGTGGTCACT Reverse Primer: ACACCTTACTCTTCATCCCTTGGA Reporter: ACCTCATGCCAGCAACT
	Katnb1-2 MD	Forward Primer: GCTGGCGCCGGAAC Reverse Primer: GCGACTATAGAGATATCAACCACTTTGT Reporter: AAGCTGGGTCTAGATATC
	Katnb1-2 EX	Forward Primer: GCGCCGGAACCGAAGT Reverse Primer: TCTGGGTTCTCAATACAGGGATGT Reporter: CTGAGCTCGCCATCAGT
	CRE	Forward Primer: TTAATCCATATTGGCAGAACGAAAACG

		Reverse Primer: CAGGCTAAGTGCCTTCTCTACA Reporter: CCTGCGGTGCTAACC

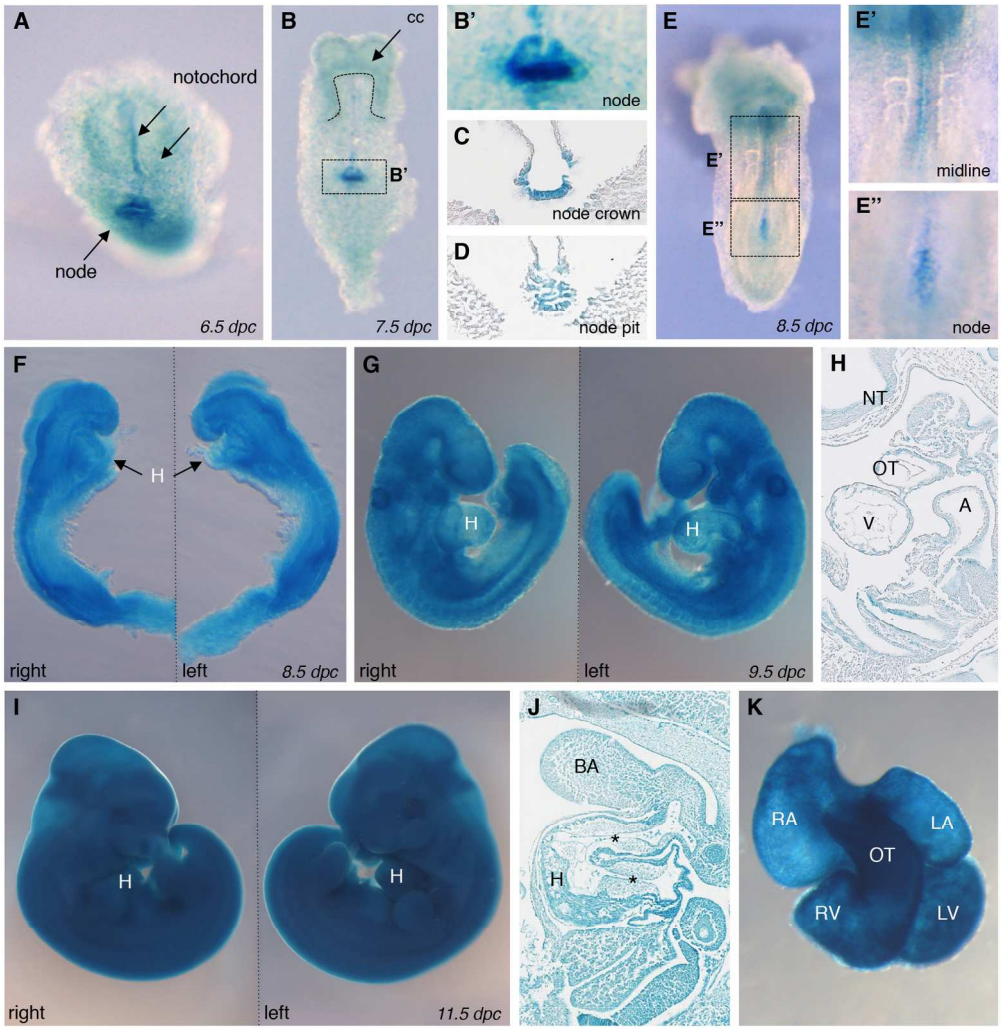

Figure 1 – Katnb1 expression in embryonic development reported by LacZ activity. A. Ventral view of a 6.5dpc embryo showing pale ubiquitous staining throughout embryo and stronger staining in the node and primitive streak areas. B. Ventral view of 7.5 dpc embryo showing pale staining in cardiac crescent (cc) area, highlighted by dashed black line, and node (boxed area). B' zoom of nodal staining. C-D. Histological sections through crown cells on the node (C) and pit region (D). E-E". Ventral view of 8.5 dpc embryo highlighting midline (E') and node (E") staining in boxed regions. F. Overnight staining of 8.5 dpc embryo highlighted the ubiquitous embryonic LacZ staining, including the heart (H). G. Ubiquitous staining was sustained to 9.5 dpc. H. Sagittal section showing ubiquitous LacZ staining in the neural tube (NT), outflow tract (OT), ventricle (V) and atrial (A) cardiac regions. I-K. Lateral views of 11.5 dpc embryo, showing ubiquitous LacZ staining was sustained at later developmental stages. J. Isolated 11.5 dpc heart showed staining in all compartments. K. Sagittal section highlighting staining in branchial arch (BA), and heart (H), including cardiac cushion material (asterisks), responsible for formation of valves and for septation.

178x183mm (300 x 300 DPI)

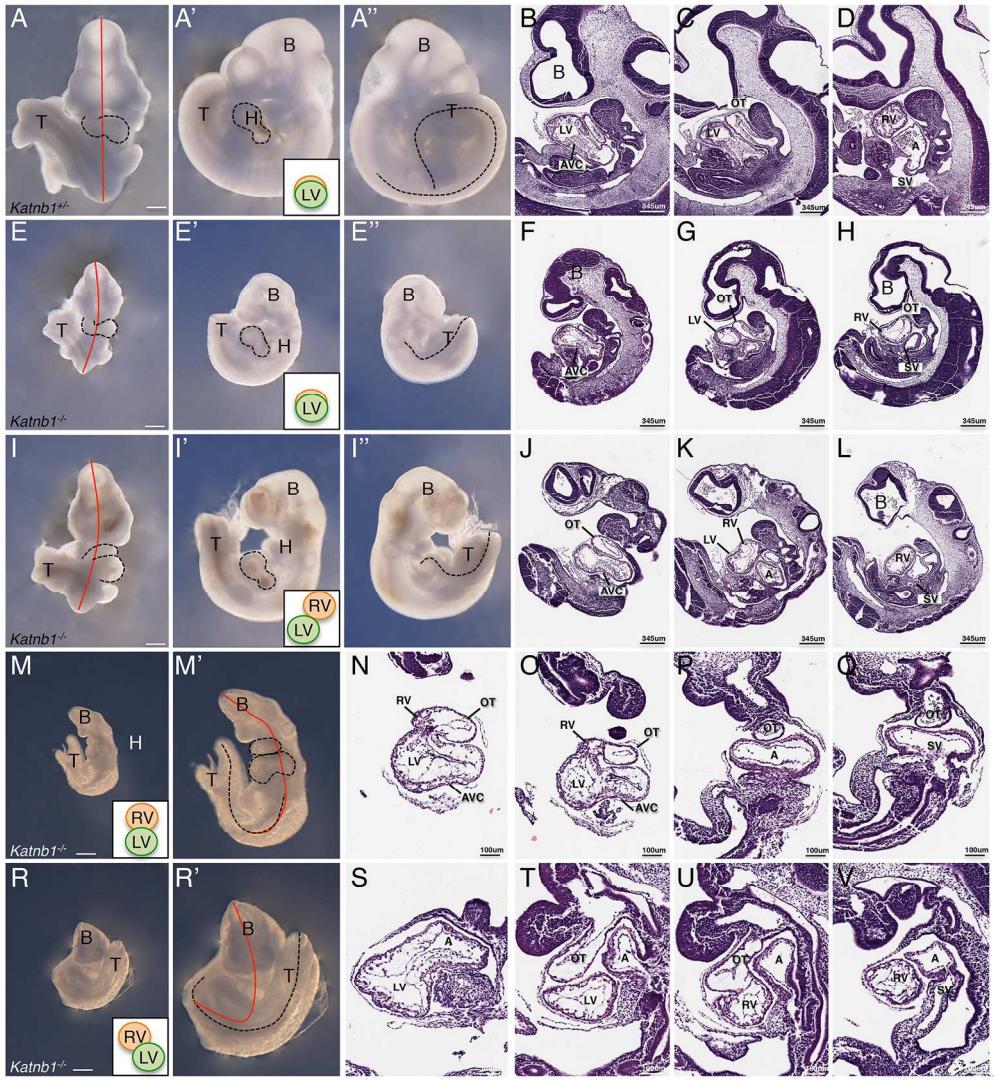

Figure 2 – Katnb1-/- embryos showed developmental delay, turning and heart looping phenotypes at 10.5dpc. A-D. Ventral (A), left-sided (A') and right-sided (A") views of control embryo showing normal development of neural tube, body axis (red line), heart (black dashed circle) and tail positioning (black dashed lines). B-D. Sagittal sections through various levels of the heart showing proper formation and positioning of cardiac chambers, including left ventricle (LV), right ventricle (RV), atrioventricular canal (AVC), atria (A), sinus venosus (SV) and outflow tract (OT). E-H. Mutant embryo displaying growth retardation (E-E"), axis (E) and tail looping (E") abnormalities but grossly normal heart looping (E', F-H). I-L. Mutant embryo showing intermediate axial (I), heart (I', J-L) and tail looping (I") abnormalities. M-V. Two mutant embryos showing severe growth retardation (M, R) and other morphogenetic defects. Closer ventral view of embryos (M', R') highlights axial rotation, as well as abnormal heart and tail looping. N-Q. Ventral sections of mutant embryo shown in M, displaying looping abnormalities. R-V. Sagittal sections through embryo shown in R, showing abnormal alignment of cardiac chambers. Insets in A', E',I',M and R show orientation of the RV in relation to the LV. A' shows correct relationship between ventricles. Katnb-/- muatn embryos show a range of looping phenotypes from correct heart loop (E') or partial heart loops (I', R) to reversal (M').
B – brain; T – tail.

175x189mm (300 x 300 DPI)

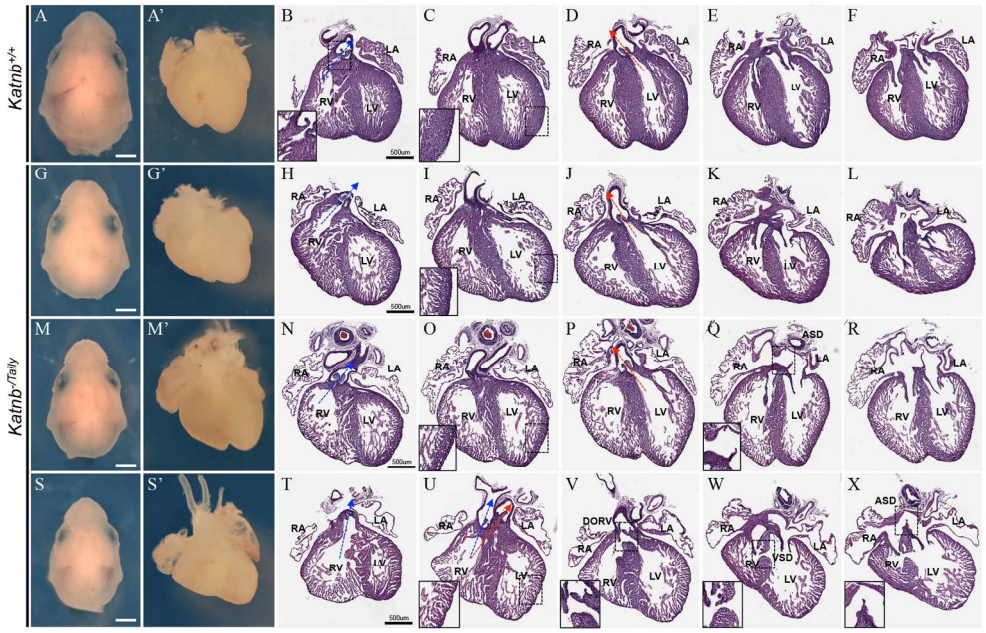

Figure 3 – Katnb-/Taily compound fetuses show cardiac abnormalities at 16.5 dpc. A, G, M, S - Head sizes highlight growth retardation in Katnb-/Taily fetuses when compared with control littermates. The genotype is indicated on the left hand side of the figure. A', G', M', S' - Whole mount view of control and compound mutant hearts (Katnb-/Taily) showing the gross morphology was not affected in most hearts. B-X - Longitudinal sections of hearts showing partially penetrant cardiac malformations in compound mutant fetuses. The range in the severity of phenotype is shown from top to bottom panels, with less severe on top (H-L). Hearts shown in panels S'-X had the most severe phenotype, consisting of double outlet right ventricle (DORV), ventricular septal defect (VSD; dashed area and inset in W) and atrial septal defect (ASD; dashed area and inset in Q, X). The blue arrows point to the direction of connection of the right ventricle (RV) with the pulmonary artery. The red arrows point to the direction of the connection between the left ventricle (LV) with the aorta, or the RV with the aorta in panel U. Dashed areas and insets in N, X point to malformed atrial or W for ventricular septa. Dashed area and inset in C show normal compact myocardium in control heart or highlights hypoplastic myocardial chambers in Katnb-/taily mutant hearts (I, O and U). RA – right atrium; LA – left atrium

175x121mm (300 x 300 DPI)

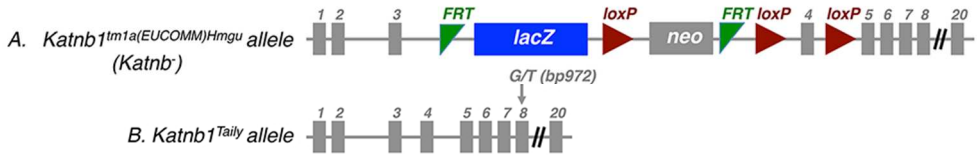

Figure 4 – Genetic map of Katnb1 allelic series used for embryonic phenotyping. A. EUCOMM engineered allele showing Flp-recombinase recognition sites (FRT) flanking a beta-galactosidase expression cassette (lacZ) and a neomycin selection cassette (neo). Three Cre-recombinase recognition sites (LoxP) allow excision of the neo cassette and/or the endogenous exon4 of the Katnb1 gene. FRT sites allow excision of lacZ and neomycin cassettes. The mice used in this manuscript have not undergone CRE or FLP mediated deletion, but the insertion of the knockin cassette causes premature termination of the gene. B. A second Katnb1 allele (Katnb1Taily) was independently modified by a point mutation in exon 8, which caused a G/T nucleotide change and conversion from valine to phenylalanine in the WD40 domain of the protein (O'Donnell et al., 2012), supposed to bind p60 and target the protein to subcellular compartments. This allele was further crossed with allele A (Katnb1-)

85x14mm (300 x 300 DPI)